Dispersion in Fluid-Filled Pipes by Analyzing Finite Element Models

Matthias Maess, Lothar Gaul
Institute A of Mechanics, University of Stuttgart, Pfaffenwaldring 9, 70550 Stuttgart, Germany
Email: {maess,gaul}@mecha.uni-stuttgart.de

Introduction

The analysis of harmonic wave propagation in pipes is of major interest in many engineering applications, such as in the field of vibro-acoustics or for non-destructive testing by using elastic waves, just to name two. Hereby, fluid-filled pipes represent a unidirectional waveguide. These guided waves are largely dispersive. The analysis of this problem has been addressed by Fuller and Fahy [2], who use an analytical model, which is solved numerically. Such analytical methods however need to be adjusted for different pipe geometries. To overcome this limitation, waveguide finite elements (WFEM) have been developed in order to numerically investigate wave propagation. Hereby, only the cross section needs to be modelled in two dimensions. However, special finite elements need to be designed and implemented. Mace et al. [3] have therefore presented a method based on postprocessing standard FE-packages in order to extract all necessary information about guided waves in flexible pipes, namely the dispersion curves as well as group velocities, phase velocities, power transmission and energy density. This methodology is applied to a water-filled brass pipe. The two-field problem is solved numerically by means of a segment FE-model as shown in Fig. 1.

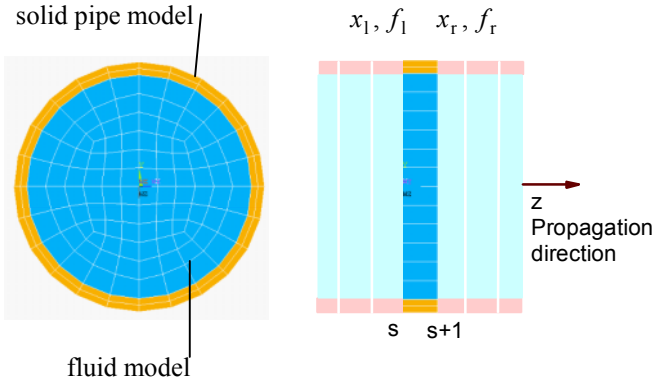

Figure 1: Segment model of the fluid-filled pipe in ANSYS.

Wave Modes by Finite Element Model

The FE-based method uses fully coupled FE-models in non-symmetric representation according to [4]

$$\begin{bmatrix} \boldsymbol{M}_{\mathrm{ss}} & \boldsymbol{0} \\ \rho \boldsymbol{Q}^T & \boldsymbol{M}_{\mathrm{ff}} \end{bmatrix} \begin{pmatrix} \ddot{\boldsymbol{u}} \\ \ddot{\boldsymbol{p}} \end{pmatrix} + \begin{bmatrix} \boldsymbol{K}_{\mathrm{ss}} & -\boldsymbol{Q} \\ \boldsymbol{0} & \boldsymbol{K}_{\mathrm{ff}} \end{bmatrix} \begin{pmatrix} \boldsymbol{u} \\ \boldsymbol{p} \end{pmatrix} = \begin{pmatrix} \boldsymbol{f}_{\mathrm{s}} \\ \boldsymbol{q}_{\mathrm{f}} \end{pmatrix}. \qquad (1)$$

Time-harmonic behaviour is assumed in the waveguide and leads to FRFs. The dynamic stiffness matrix with inclusion of viscous damping model represented by $\boldsymbol{C}$ is given by

$$\boldsymbol{H}(\omega)\boldsymbol{x}(\omega) = \boldsymbol{f}(\omega), \quad \boldsymbol{H}(\omega) = \boldsymbol{K} + j\omega\boldsymbol{C} - \omega^2\boldsymbol{M}\,. \qquad (2)$$

Following Mace et al. [3], the DOFs are resumed as $\boldsymbol{x} = [\boldsymbol{u}^T\ \boldsymbol{p}^T]^T$, $\boldsymbol{f} = [\boldsymbol{f}_{\mathrm{s}}^T\ \boldsymbol{q}_{\mathrm{f}}^T]^T$ and partitioned according to left and right position on the pipe segment, i.e. $\boldsymbol{x} = [\boldsymbol{x}_{\mathrm{l}}^T\ \boldsymbol{x}_{\mathrm{r}}^T]^T$ $\boldsymbol{f} = [\boldsymbol{f}_{\mathrm{l}}^T\ \boldsymbol{f}_{\mathrm{r}}^T]^T$, see Fig. 1. The order has to match corresponding positions in longitudinal direction. On the interface, continuity of Dirichlet data $\boldsymbol{x}_{\mathrm{l}}^{s+1} = \boldsymbol{x}_{\mathrm{r}}^{s}$ and of the Neumann data $\boldsymbol{f}_{\mathrm{l}}^{s+1} = -\boldsymbol{f}_{\mathrm{r}}^{s}$ is imposed. Afterwards, rearrangement leads to

$$\begin{pmatrix} \boldsymbol{x}_{\mathrm{l}}^{s+1} \\ \boldsymbol{f}_{\mathrm{l}}^{s+1} \end{pmatrix} = \underbrace{\begin{bmatrix} -\boldsymbol{H}_{\mathrm{lr}}^{-1}\boldsymbol{H}_{\mathrm{ll}} & \boldsymbol{H}_{\mathrm{lr}}^{-1} \\ -\boldsymbol{H}_{\mathrm{rl}} + \boldsymbol{H}_{\mathrm{rr}}\boldsymbol{H}_{\mathrm{lr}}^{-1}\boldsymbol{H}_{\mathrm{ll}} & -\boldsymbol{H}_{\mathrm{rr}}\boldsymbol{H}_{\mathrm{lr}}^{-1} \end{bmatrix}}_{\boldsymbol{T}} \begin{pmatrix} \boldsymbol{x}_{\mathrm{l}} \\ \boldsymbol{f}_{\mathrm{l}} \end{pmatrix} \qquad (3)$$

Since wave modes propagate in z-direction at the s-th element layer as $\boldsymbol{x}_{\mathrm{l}}^{s+1} = \mathrm{e}^{\kappa z}\boldsymbol{x}_{\mathrm{l}}$ and $\boldsymbol{f}_{\mathrm{l}}^{s+1} = \mathrm{e}^{\kappa z}\boldsymbol{f}_{\mathrm{l}}$ with complex longitudinal wave number κ, an eigenproblem is formulated and solved numerically

$$T\begin{pmatrix} \hat{\boldsymbol{x}}_{\mathrm{l}} \\ \hat{\boldsymbol{f}}_{\mathrm{l}} \end{pmatrix} = \lambda \begin{pmatrix} \hat{\boldsymbol{x}}_{\mathrm{l}} \\ \hat{\boldsymbol{f}}_{\mathrm{l}} \end{pmatrix} \quad \text{with} \quad \lambda = \mathrm{e}^{\kappa z}\,. \qquad (4)$$

From the eigenpairs, wave numbers and wave mode shapes are recovered. Dispersion curves are represented in Fig. 2. Frequencies are normalized with respect to the ring frequency $\Omega = \omega / \omega_r$ of the in vacuo-pipe and wave numbers by multiplication with mean radius a [2].

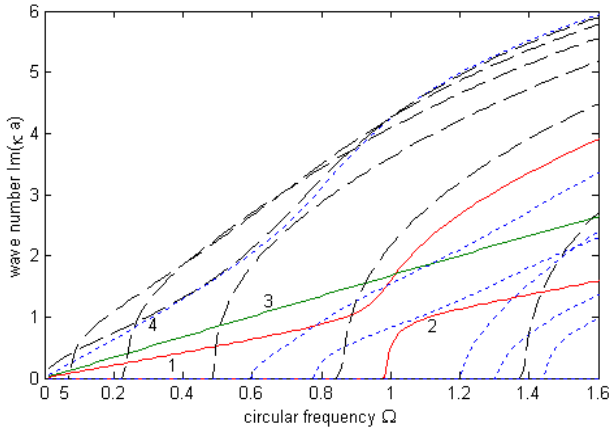

Figure 2: Dispersion curves. (- - - bending modes, … fluid-type modes, ---- solid-type modes)

The branches are further postprocessed to obtain phase velocities and group velocities respectively

$$c_p = \frac{\omega}{\kappa} \qquad c_g = \frac{\partial \omega}{\partial \kappa}. \tag{5}$$

However, retrieving the group velocity by differentiating dispersion curves involves numerical errors, therefore the group velocities are computed as

$$c_g = \frac{P}{\overline{E}} = \frac{P_f + P_s}{\overline{T}_s + \overline{U}_s + \overline{T}_f + \overline{U}_f}. \tag{6}$$

Hereby, $\overline{E}$ denotes the time-averaged energy density per unit length, whereas P_s and P_f represent power flow over solid and fluid cross section respectively. The kinetic energy densities are computed from the eigenvectors as

$$\overline{T}_s = \frac{1}{4\Delta l}\omega^2 \hat{\boldsymbol{u}}^H \boldsymbol{M}_{ss} \hat{\boldsymbol{u}} \quad \overline{T}_f = \frac{1}{4\Delta l \rho \omega^2} \hat{\boldsymbol{p}}^H \boldsymbol{K}_{ff} \hat{\boldsymbol{p}}, \tag{7}$$

and potential energy densities as

$$\overline{U}_s = \frac{1}{4\Delta l} \hat{\boldsymbol{u}}^H \boldsymbol{K}_{ss} \hat{\boldsymbol{u}} \quad \overline{U}_f = \frac{1}{4\Delta l \rho} \hat{\boldsymbol{p}}^H \boldsymbol{M}_{ff} \hat{\boldsymbol{p}}. \tag{8}$$

Time-averaged power flow rates are given by

$$P_s = \frac{1}{2}\omega \Im\left\{ \hat{\boldsymbol{f}}_{s,l}^{H} \hat{\boldsymbol{u}} \right\} \quad P_f = \frac{1}{2\rho\omega} \Im\left\{ \hat{\boldsymbol{q}}_{f,l}^{H} \hat{\boldsymbol{p}}_l \right\}. \tag{9}$$

The group velocities according to (6) are given in Fig. 3 for the water-filled brass pipe.

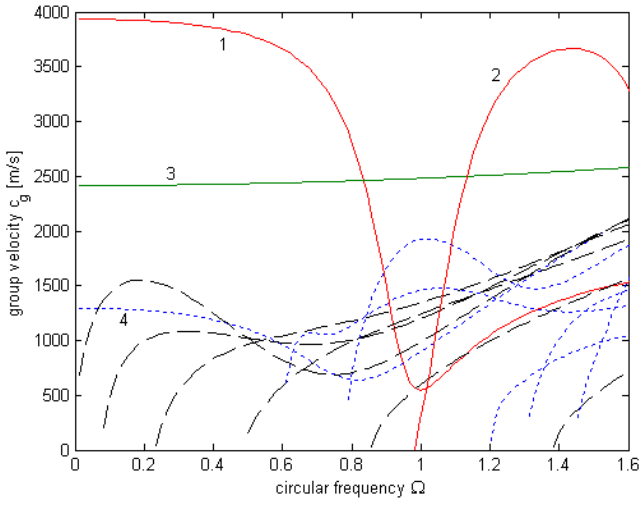

Figure 3: Modal group velocities.

Results

Computations are performed for a water-filled brass pipe with $R_i = 0.034\text{m}$, $R_a = 0.038\text{m}$ by means of a segment FE-model with 674 DOFs (Fig. 1). The model is assembled by hexahedral solid and fluid elements. The length of the pipe segment is chosen as $\Delta l = 1\,\text{cm}$. Wave modes are identified in the dispersion diagram (Fig. 2). Circumferential (n) and radial (kr) modal orders classify propagating wave modes [2]. At low frequencies, only one beam-type bending mode (n=1), one torsional mode (n=0, branch 3), one longitudinal extensional-type wave (branch 1) and one fluid-type mode (branch 4) occur. Near the ring frequency, n=0-modes show strong dispersion, and a further longitudinal mode cuts on (branch 2). Higher-order bending modes (- - -) cut on such as at $\Omega = 0.07\,\text{Hz}$ (n=2) and $\Omega = 0.23$ (n=3). Higher-order fluid-type waves (⋯) exist above cut-on frequencies, for example at $\Omega = 0.59\,\text{Hz}$ (n=1,kr=0) and $\Omega = 0.77\,\text{Hz}$ (n=2,kr=0). The results show very good agreement with solutions of analytical fluid-shell models by Fuller and Fahy [2].

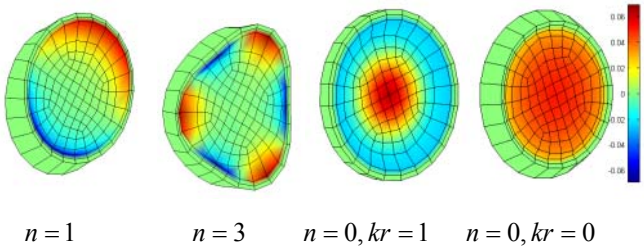

Figure 4: Wave modes, displacement and acoustic pressure.

Wave modes can be illustrated as shown in Fig. 4 for bending modes (n=1,n=3) and fluid-type modes (n=0, kr=1) and (n=0, kr=1) cutting on at $\Omega = 1.65\,\text{Hz}$. The usefulness of the method from Mace et al. [3] is modified for the acoustic two-field problem in pipes and shows excellent results. By using standard FE-package, it eases very fast and flexible modelling. Various kinds of linear FE-models may be included. Results may be used for NDE purposes, vibro-acoustic system excitation and power transmission as well as for designing models for Transfer Matrix Methods (TMM).

Acknowledgements

Funding of this project by the German Research Society DFG in the Collaborative Research Center SFB 412 “Computer Aided Modeling and Simulation for Analysis, Synthesis and Operation in Process Engineering” is gratefully acknowledged.

References

[2] Finnveden, S.; Nilsson, C.-M.: Waveguide finite elements for fluid-shell coupling. *International Conference on Sound and Vibration,* Stockholm, 2003, 3271-3278.

[2] Fuller, C. H.; Fahy, F.J.: Characteristics of wave propagation and energy distribution in cylindrical elastic shells filled with fluid. *Journal of Sound and Vibration* **81**(4),501-518,1982.

[3] Mace, B.R; Duhamel, D.; Brennan, M.J.; Hinke, L.: Wavenumber prediction using Finite Element analysis, In: *International Conference on Sound and Vibration,* St. Petersburg, 2004, 3241-3248.

[4] Zienkiewicz, O.C.; Taylor, R.L.: *The Finite Element Method*, Butterworth-Heinemann, Oxford, 2002.